

Visualization of wavefront aberrations by Zernike polynomials

Stephan Reichelt^{1*}

¹ Institute of Applied Optics (ITO), University of Stuttgart, Pfaffenwaldring 9, 70569 Stuttgart, Germany

Abstract – Zernike aberration coefficients are typically presented in tabular form or as simple bar graphs, making it difficult to intuitively interpret their meaning and relate them to the specific aberration term. In this work, we present intuitive and rapidly interpretable visual representations of Zernike aberration terms that highlight the magnitude and orientation of their dominant contributions. Depending on the aberration order, we recommend different graphical formats – such as bubble plots and heatmaps – for visualizing low-order and mid-spatial frequency Zernike terms. These graphical representations are particularly valuable when quick visual feedback on individual aberration terms is needed, such as during aberration compensator adjustment, real-time wavefront visualization of dynamic processes, or optical alignment procedures. They can also enhance the clarity and interpretability of inspection reports or measurement certificates. Furthermore, an alternative definition of the azimuthal orientation of Zernike terms with $m \neq 0$ is proposed, enabling a more effective analysis of the shape and bending of spoke-shaped aberrations.

Keywords. Zernike polynomials, Visualization, Wavefront analysis, Wavefront aberrations, Optical testing

1. Introduction

Polynomial sets such as Zernike polynomials [1–4] are widely used in various applications to approximate optical aberrations in a compact and sufficiently accurate manner. For example, in precision optical manufacturing, Zernike polynomials are used to characterize and approximate surface figure errors of optical components (e.g., lenses, flats) or wavefront aberrations of optical systems measured by interferometers or wavefront sensors. Freeform surfaces, which can also be described by Zernike polynomials, play an important role in optical design. In addition, Zernike polynomials are typically used in adaptive optics to compensate for dynamic aberrations, such as those caused by atmospheric turbulence.

The present work is motivated by the aim of providing a representation of Zernike approximation results that is as simple and intuitive as possible. Conventional formats such as tabular listings or bar plot visualizations, while widely used, often fail to adequately convey structural relationships and limit the direct interpretability of the underlying wavefront or surface characteristics. For users working with Zernike polynomial representations in optical design, metrology, or ophthalmology, the interpretation of coefficient sets can be non-trivial, particularly in the presence of multiple interacting modes or when spatial patterns must be inferred indirectly. This can make it difficult to extract relevant insights efficiently, even for

experienced practitioners. To address this, the present work introduces a novel representation that is specifically designed to make structurally relevant features more directly accessible, thereby facilitating interpretation and supporting more effective analysis of Zernike-based wavefront or surface descriptions.

2. Definition of Zernike polynomials

Figure 1 illustrates the first 15 Zernike polynomials, arranged in a pyramid up to the 4th order.

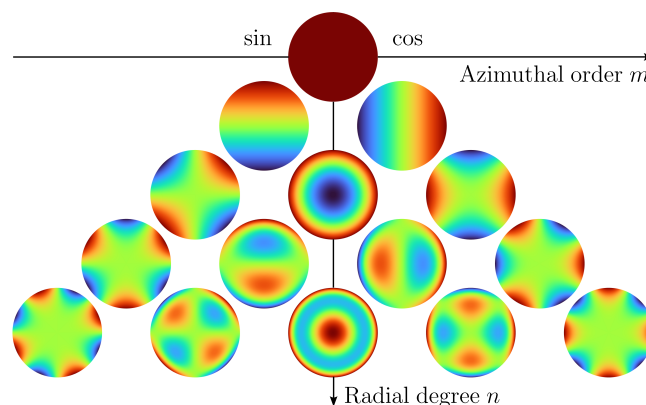


Figure 1: Pyramid representation of the non-normalized Zernike polynomials Z_n^m up to the 4th order.

* Corresponding author: reichelt@ito.uni-stuttgart.de

36 Zernike polynomials are expressed either in Cartesian
 37 (x, y) or conveniently in polar coordinates (r, θ) . They are
 38 defined within the unit circle, where r is the normalized
 39 radial distance from the origin, and θ is the angle from the
 40 x axis (common right-handed coordinate system). Apart
 41 from a preceding normalization factor N_n^m , Zernike poly-
 42 nomials are the product of a radial polynomial $R_n^m(r)$ and
 43 an azimuthal function $M_m(\theta)$

$$Z_n^m(r, \theta) = N_n^m \cdot R_n^m(r) \cdot M_m(\theta), \quad (1)$$

44 where n is the degree of the polynomial and m is the az-
 45 imuthal dependence parameter [2, 5]. The azimuthal order
 46 m is an integer ($m \in \mathbb{Z}$), whereas the polynomial de-
 47 gree or radial order n is a non-negative integer ($n \in \mathbb{N}_0$).
 48 For a particular Zernike polynomial Z_n^m , the integral val-
 49 ues n and m are either both even or both odd. **The double-**
 50 **indexing scheme, in which n denotes the highest power**
 51 **of the radial polynomial and m the azimuthal order, is**
 52 **essential for unambiguously describing the Zernike poly-**
 53 **nomials.**

54 The radial polynomials $R_n^m(r)$ are explicitly defined
 55 by

$$R_n^m(r) = \sum_{s=0}^{\frac{n-|m|}{2}} \frac{(-1)^s (n-s)!}{s! (\frac{n+m}{2} - s)! (\frac{n-m}{2} - s)!} r^{n-2s}, \quad (2)$$

56 whereas the azimuthal function $M_m(\theta)$ is given by¹

$$M_m(\theta) = \begin{cases} -\sin(m\theta) & \text{for } m < 0 \\ \cos(m\theta) & \text{for } m \geq 0 \end{cases}. \quad (3)$$

57 Optionally, a normalization factor N_n^m may be ap-
 58 plied, defined as

$$N_n^m = \begin{cases} 1 & \text{for no normalization} \\ \sqrt{(2 - \delta_{m0})(n+1)} & \text{for RMS normalization} \end{cases} \quad (4)$$

59 where δ_{m0} is the Kronecker delta function.² If the normal-
 60 ization factor N_n^m is set to 1, the Zernike polynomials are
 61 referred to as non-normalized, implying that either their
 62 maximum is 1 or that their maximum and minimum are
 63 ± 1 , respectively. In contrast, for RMS-normalized poly-
 64 nomials, the normalization factor is defined such that the
 65 root-mean-square (RMS) value of each polynomial is 1.
 66 This ensures that, when a polynomial fit is applied to
 67 a data set, the **absolute value $|c_n^m|$ of the fitted Zernike**
 68 **coefficients directly represent the RMS values of the as-**
 69 **sociated aberration terms.** For numerical reasons, it is
 70 advantageous to apply the RMS normalization not to the
 71 Zernike polynomials themselves, but to the coefficients
 72 obtained from the fit.

73 **Note that each Zernike polynomial pair, Z_n^m and Z_n^{-m}**
 74 **(for $m \neq 0$), has the same normalization factor $N_n^m =$**
 75 **N_n^{-m} as well as the same radial polynomial $R_n^m(r) =$**
 76 **$R_n^{-m}(r)$.**

¹ Note that the sine function is an odd function where $\sin(-x) = -\sin(x)$. For $m < 0$, the negative sign of the sine function is necessary for a correct notation.

² Kronecker delta is defined as $\delta_{m0} = \begin{cases} 1 & \text{for } m = 0 \\ 0 & \text{for } m \neq 0 \end{cases}$.

3. Sample wavefront data

77

78 Two representative wavefronts are employed to il-
 79 lustrate the visualization methods discussed in this pa-
 80 per. Wavefront A (Fig. 2) corresponds to the measured
 81 aberrations of a lens surface, containing both low- and
 82 mid-spatial frequency contributions, while wavefront B
 83 (Fig. 3) is synthetically generated to highlight the orien-
 84 tation of individual azimuthal orders.

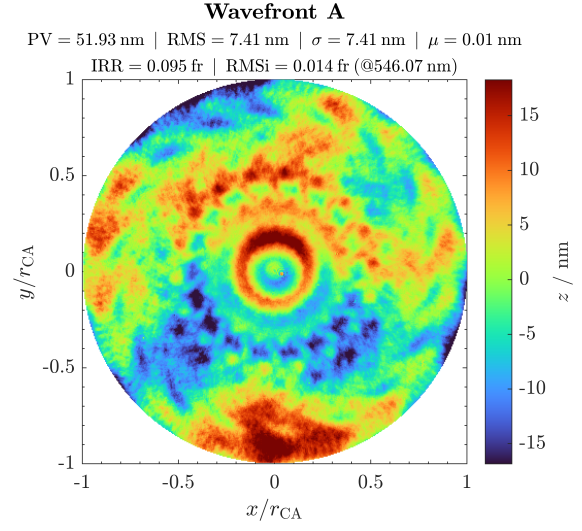


Figure 2: Sample wavefront A: measurement data of a lens surface.

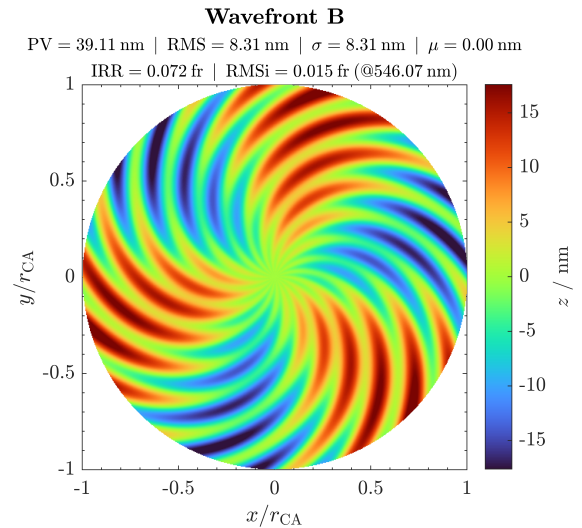


Figure 3: Sample wavefront B: synthetic aberration data.

84

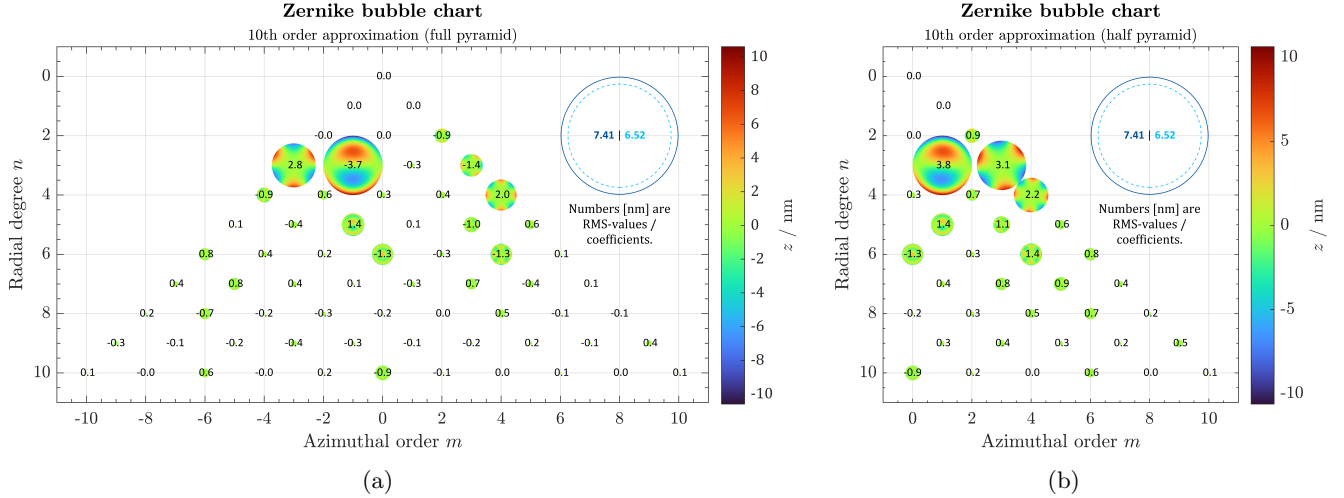


Figure 4: Bubble chart plots of low-order Zernike aberration coefficients in full-pyramid representation (a) and in half-pyramid representation (b). The area of the depicted aberration terms (bubble size) is proportional to the magnitude of its RMS-normalized Zernike coefficient c_n^m . The blue circles on the upper right represent the areas of the total RMS-deviation of the wavefront error (dark blue) and its fitted RMS-deviation by the shown low-order aberrations fit of a 10th order polynomial (light blue). The numbers within the pyramid represent the RMS-normalized Zernike coefficients [nm], whereas the numbers in the blue reference circles (upper right corner) are the RMS-values [nm] of the original wavefront and its fitted 10th-order counterpart. Primary coma and trefoil are the main aberration terms.

85 4. Representing low-order Zernike 86 aberrations

87 Often, the coefficients resulting from a least-squares
88 Zernike fit are presented in tabular form or as simple bar
89 graphs using a single-indexing scheme. However, Zernike
90 polynomials depend on two integer parameters, n and m ,
91 which makes any single-indexing scheme arbitrary. This
92 makes it difficult to interpret their meaning and relate
93 them to the specific aberration term, especially since dif-
94 ferent single-index ordering schemes are in use, such as
95 ANSI/ISO 24157, Born/Wolf, Standard, or Fringe.

96 Evans et al. [6] proposed a graphical representation,
97 showing the magnitude of the various Zernike orders in
98 dependence of the azimuthal order m and the degree n of
99 the radial polynomial, a method that was adopted by the
100 author years ago for plotting the aberration coefficients
101 as two-dimensional bar plots, e.g. in [7].

102 Inspired by this, an even more intuitive way for rep-
103 resenting low-order Zernike aberration coefficients is pro-
104 posed here. It makes use of the Zernike pyramid and the
105 fact, that the RMS-normalized Zernike coefficients are un-
106 correlated to each other. Hence, the root-sum-of-squares
107 (rss) level of individual RMS-normalized Zernike coeffi-
108 cients c_n^m yields the total RMS-value of the aberration

$$\text{RMS}_{\text{total}} = \sqrt{\sum_{i=1}^{\infty} \text{RMS}_i^2} = \sqrt{\sum_{i=1}^{\infty} (c_n^m)_i^2}. \quad (5)$$

109 The basic idea is just use a bubble plot depiction of
110 the Zernike pyramid and scale the size of each individ-
111 ual bubble (or individual Zernike polynomial) with the
112 magnitude of the RMS-normalized Zernike coefficient c_n^m .

113 There is a physical meaning in this scaling as the sum of
114 all individual bubble areas corresponds to the total RMS-
115 value. By way of example this is shown in Fig. 4(a) for an
116 X/Y representation of the full Zernike pyramid.

117 Here, the total RMS deviation of sample wavefront A
118 having 7.41 nm is taken as the reference area (area \propto
119 $\text{RMS}_{\text{total}}^2 \propto r_{\text{total}}^2$, cf. dark blue circle in the up-
120 per right corner). The individual radii scale then with
121 $|c_n^m|_i / \text{RMS}_{\text{total}}$, i.e. the total area of all shown bubbles
122 (10th order fit with 66 polynomials) therefore corresponds
123 to the light blue dotted area $\propto \text{RMS}_{10\text{th}}^2 = (6.52 \text{ nm})^2$.
124 It can be easily seen in Fig. 4(a) that primary Y -coma and
125 primary Y -trefoil are the main aberration contributors.
126 An advantage of the full pyramid or X/Y representation
127 is that the signs of the Zernike coefficients c_n^m are pre-
128 served, either through the positions of the maxima and
129 minima of the individual Zernike terms or through addi-
130 tional numerical annotation.

131 Another, even more convenient depiction is a
132 Mag/Angle representation utilizing only half of the
133 Zernike pyramid, see Fig. 4(b). The magnitude of the
134 paired X/Y coefficients is given by

$$|c_n^m| = \sqrt{(c_n^{-m})^2 + (c_n^{+m})^2}, \quad (6)$$

135 whereas the angular orientation results just from adding
136 up $(c_n^{-m} Z_n^{-m} + c_n^{+m} Z_n^{+m})$ pairwise. Magnitude and ori-
137 entation can be then interpreted intuitively.

138 Note that in Fig. 4, the terms piston, tilt, and defo-
139 cus have been set to zero intentionally, since they de-
140 scribe alignment parameters rather than intrinsic surface
141 or wavefront aberrations.

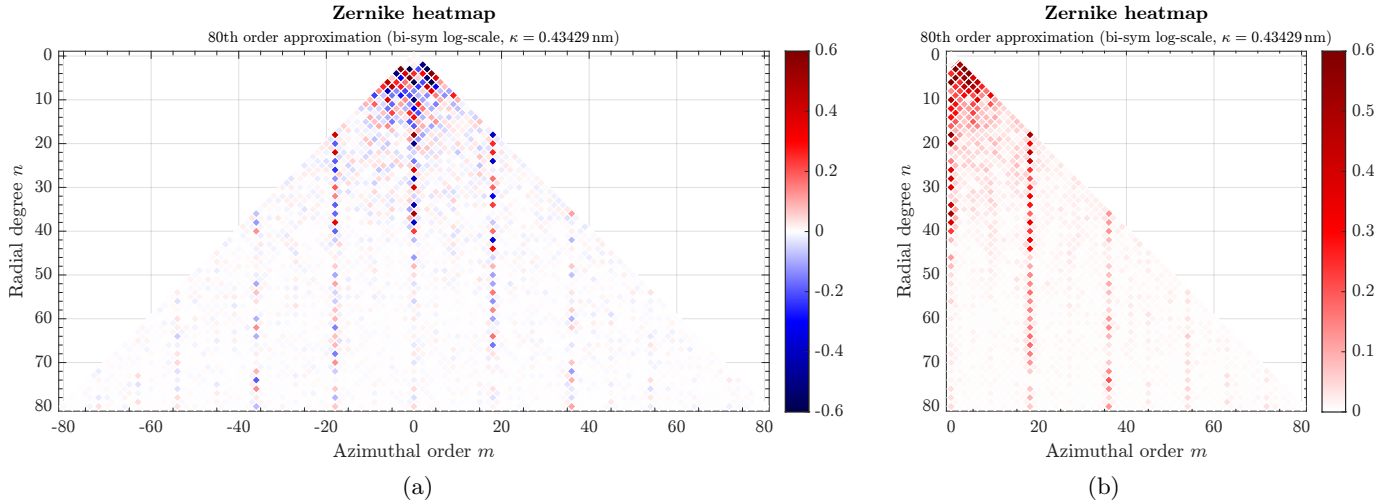


Figure 5: Heatmaps of Zernike aberration coefficients for a 80th-order approximation in full-pyramid representation (a) and in half-pyramid representation (b). To emphasize coefficients with small magnitudes, the coefficients are displayed on a bi-symmetric logarithmic scale [8]. In the full-pyramid representation, the signs of the coefficients are preserved, whereas in the half-pyramid representation, the magnitudes of the respective coefficient pairs are shown.

5. Representing mid- and high-spatial frequency Zernike terms

Whereas the Zernike pyramid representation with scaled bubbles is adequate for visualizing polynomial degrees up to the 10th or 12th order, it becomes impractical for high-order fits. Zernike coefficient maps (also called Zernike spectra) are ideally suited for this purpose.

Figure 5 presents heatmaps of Zernike aberration coefficients obtained from a 100th-order fit of sample wavefront A. To emphasize coefficients with small magnitudes, the data are displayed using a bi-symmetric logarithmic scale [8]. The scaling constant of the bi-symmetric transfer function, which controls the slope near the origin, was set here to $\kappa = 1/\ln(10)$ nm.

Note that the heatmaps are not displayed as a conventional pixel grid, but instead as a square tiling rotated by 45° and rendered using patches. This representation avoids gaps in the spectrum and ensures that the pyramid is fully filled. Alternative spectral representations [9, 10] employ a modified radial index n_F for the same purpose, namely to circumvent such gaps. The representation presented here simultaneously provides a fully filled pyramid while preserving the conventional ordering of the radial polynomial degree n along the ordinate.

The log-based representation clearly reveals characteristic azimuthal orders with $m = 18$ and their higher harmonics ($m = 36, 54, 72$) in the wavefront. The heatmaps therefore reveal specific mid-spatial-frequency errors, such as ripple and spoke-like structures. Rotationally variant irregularities, or spoke-shaped aberrations, represent a specific form of surface undulations characterized by regular azimuthal orders extending toward the origin of the wavefront map. Such azimuthal waviness is typically introduced by manufacturing processes involving rotational motion about the workpiece

center. Examples include precision contour grinding of lenses, where chatter marks may arise from ring tools, as well as diamond turning or direct laser beam writing using air-bearing spindles, where slight imbalances can cause run-out errors.

6. Azimuthal orientation

The angular or azimuthal orientation refers to the angle with respect to the positive x -axis at which the aberration occurs. For example, combining equal positive tilts in the x - and y -directions produces a resultant tilt oriented at $+45^\circ$. For a tilt, the direction of the aberration is unambiguous when referenced to its maximum. However, once the radial polynomial contains more than one term, local maxima or minima arise along the radial profile. How, for example, should the orientation of primary coma (cf. Fig. 6, center) be specified? Two approaches can be considered. One may, for instance, refer to the maximum value at the edge of the aperture, i.e. at $r = 1$ (previous definition). Alternatively, one may refer to the first local maximum in radial direction, which for primary coma occurs at the radius $r = \sqrt{2}/3 \approx 0.471$ (proposed definition). These two variants are discussed in more detail in the following.

In Evans et al. [6] an equation and procedure to determine the first peak in *angular* direction at the edge of the aperture (i.e. at radius $r = 1$) is derived, which further simplifies with the atan2-function to

$$\theta_0^{\text{lp}} = \frac{1}{m} \text{atan2}(c_n^{-m}, c_n^m), \quad (7)$$

where $m \in \mathbb{N}$. This variant is referred to here as the previous definition. The angular offset angle is denoted hereafter by the superscript 'lp' which stands for 'last peak in radial direction'. As can be seen from Fig. 1, for all

208 Zernike polynomials with a cosine azimuthal dependence
 209 ($m > 0$, right side of pyramid) this last peak in radial
 210 direction at $r = 1$ is always located on the positive x -axis
 211 (at $x = 1, y = 0$).

212 Here, we define another angle θ_0^{fp} for the angular ori-
 213 entation, the one that points to the first local peak in
 214 the radial direction (proposed definition). The difference
 215 is illustrated in Fig. 6.

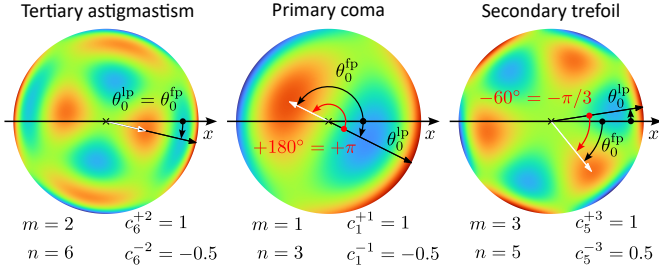


Figure 6: Comparison of the definitions for azimuthal orientation of $\pm m$ -paired Zernike polynomials. The angular orientation of the Zernike polynomials $Z_n^{\pm m}$ is illustrated for different choices of θ_0 (black arrow: common definition θ_0^{lp} ; white arrow: proposed new definition θ_0^{fp}). Left: tertiary astigmatism $Z_6^{\pm 2}$ with peaks at same azimuthal orientation. Middle: primary coma $Z_3^{\pm 1}$, where $\pi = 180^\circ$ has to be added. Right: secondary trefoil $Z_5^{\pm 3}$, where $\pi/3 = 60^\circ$ must be subtracted.

216 If $(n \bmod 4) = (m \bmod 4)$, then there is no difference
 217 in the definition. However, in all other cases (i.e., for every
 218 second diagonal wing pair of the Zernike pyramid, begin-
 219 ning with the primary coma pair), a special treatment is
 220 required. π/m must either be added or subtracted, de-
 221 pending on the signs of the coefficient pair, i.e.

$$\theta_0^{\text{fp}} = \begin{cases} \theta_0^{\text{lp}} & \text{if } (n \bmod 4) = (m \bmod 4) \\ \theta_0^{\text{lp}} + \frac{\pi}{m} & \text{elseif } (c_n^{-m} < 0) \vee (c_n^{-m} = 0 \wedge c_n^m > 0) \\ \theta_0^{\text{lp}} - \frac{\pi}{m} & \text{elseif } (c_n^{-m} > 0) \vee (c_n^{-m} = 0 \wedge c_n^m < 0) \end{cases} \quad (8)$$

222 The three conditions can be combined into a compact
 223 formula suitable for implementation

$$\theta_0^{\text{fp}} = \frac{1}{m} \text{atan2}(c_n^{-m}, c_n^m) - \frac{\pi}{m} \{[(n-m) \bmod 4] \neq 0\} \text{sign}[\text{atan2}(c_n^{-m}, c_n^m)], \quad (9)$$

224 where the first term corresponds to Eq. (7), the bracketed
 225 factor $\{.\}$ represents a logical flag $[0, 1]$ to distinguish the
 226 cases, and the sign-function determines whether π/m is
 227 added or subtracted.

228 The alternative definition of the azimuthal orientation
 229 of Zernike polynomials with $m \neq 0$ is motivated by the
 230 aim of enabling a more effective analysis of spoke-shaped
 231 aberrations. Consider the synthetically generated sample
 232 wavefront B (Fig. 3), which contains rotation-invariant

aberration components only and is composed of spoke-
 233 shaped aberrations with azimuthal orders $m = 3$ (straight
 234 spokes) and $m = 18$ (bended spokes). The angular ori-
 235 entation of the straight, spoke-shaped trefoil in sample
 236 wavefront B is compared for both definitions in Fig. 7.
 237 According to the previous definition (θ_0^{lp} as defined in
 238 Eq. (7), shown as red dashed arrows), the angle is ro-
 239 tated by π/m for every second occurrence of the poly-
 240 nomial degree n (i.e. $n = 5, 9, 13, \dots$). In contrast, under the
 241 proposed definition (θ_0^{fp} according to Eq. (9), shown as
 242 light blue arrows), the angular orientation always points
 243 in the same direction (here -45°). This makes it possible
 244 to trace the radial progression of the spokes, as shown for
 245 this example in Fig. 9(a) for the trefoil with $m = 3$.
 246

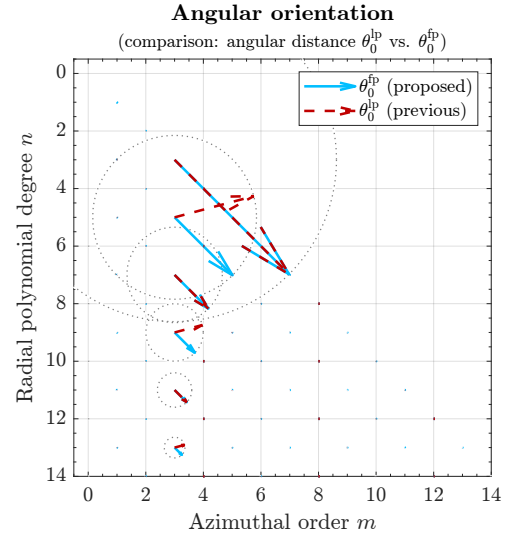


Figure 7: Comparison of the two definitions for angular orientation. The vector length represents the magnitude of the Zernike coefficient $|c_n^m|$, and the angle represents its orientation.

To analyze the bending or the shape of the spokes, rep-
 247 resentations other than the phasor plot in Fig. 7 are more
 248 suitable. First, dominant azimuthal orders are identified
 249 by applying a threshold to the root-sum-square combina-
 250 tion of the coefficients of a given order m . To plot the de-
 251 termined angles θ_0^{fp} as a function of radius, or to directly
 252 visualize their variation within the circular aperture, the
 253 radial coordinate of the first local maximum is required
 254 (cf. the endpoints of the white arrows in Fig. 6). This ra-
 255 dius is determined numerically by searching for the first
 256 extremum of the corresponding radial polynomial R_n^m .
 257 The values are computed once and stored in a look-up
 258 table.
 259

Note that the angle θ_0 in both Eqs. (7) and (8) is con-
 260 fined to a circular sector spanning the arc $0 \pm \pi/m$. With
 261 increasing m , this minor sector becomes progressively
 262 smaller. As a consequence, owing to the arctan function,
 263 the evaluated angle θ_0 is wrapped modulo $2\pi/m$. To con-
 264 sistently trace the trajectory of a spoke from the aperture
 265

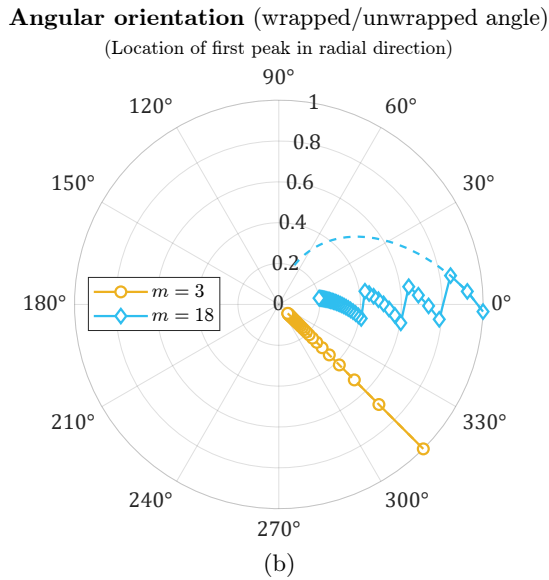
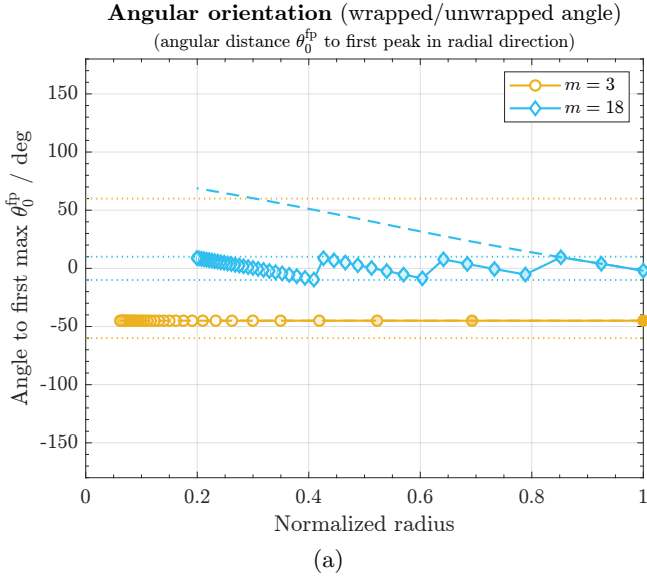


Figure 8: Visualization of the proposed definition for azimuthal orientation. (a) Angle $\theta_0^{\text{fp}}(r(n), m)$ over the radius where the first peak in radial direction occurs. (b) Polar plot of the same data.

266 rim toward the coordinate origin, it can therefore be ad-
267 vantageous to unwrap the initial angle θ_0 .

268 Figure 8 illustrates the proposed definition of the angle
269 θ_0^{fp} , shown in (a) as a function of the radius and in (b) as
270 a polar plot over the circular aperture.

271 The dominant azimuthal orders ($m = 3$ and $m = 18$)
272 of sample wavefront B are presented, including both the
273 wrapped angle (solid line with markers) and the un-
274 wrapped angle (dashed line without markers). Since, for
275 $m = 3$, the wrapped angle never reaches the limit of
276 uniqueness (indicated by the dotted line), the wrapped
277 and unwrapped angles are here identical. The representa-
278 tion in Fig. 8(a) reveals the radial dependence of the spoke

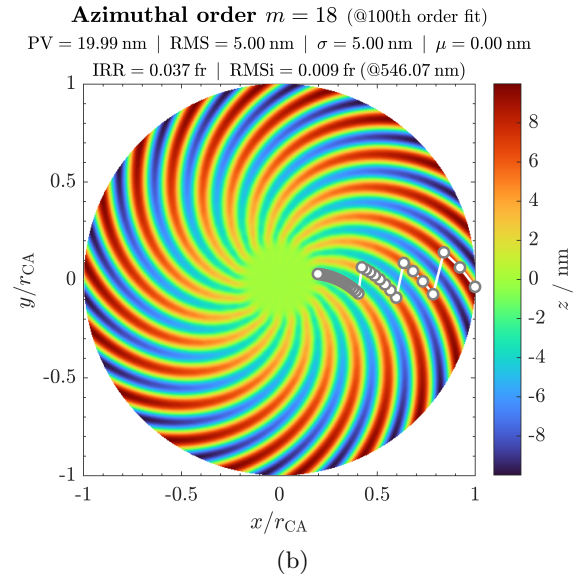
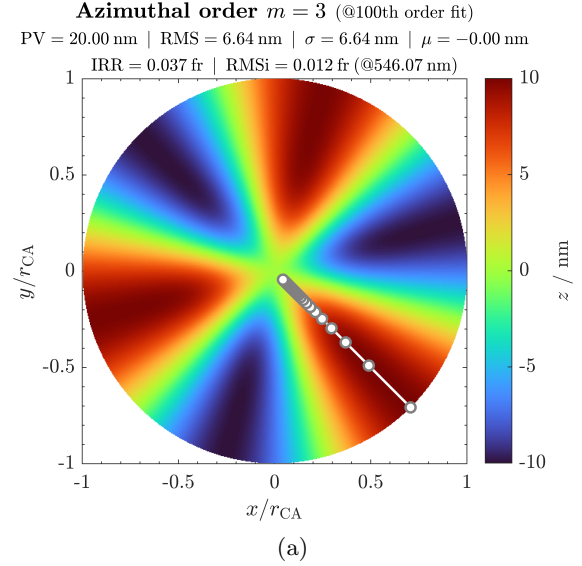


Figure 9: Zernike-fit decomposition of the azimuthal orders of sample wavefront B, overlaid with the trajectory of the unwrapped angle θ_0^{fp} . A 100th-order Zernike fit was applied, with panel (a) showing the azimuthal order $m = 3$ and panel (b) showing $m = 18$.

279 bending. For $m = 3$, the bending is constant (straight
280 spokes), whereas for $m = 18$ it exhibits a linear dependence
281 on the radius. The polar plot in Fig. 8(b) provides a
282 convenient representation for tracing the trajectory of
283 a single spoke of a given azimuthal order.

284 Finally, Fig. 9 illustrates the fitted dominant orders
285 (i.e., the sum of all Zernike terms with the same m),
286 overlaid with the trajectory of the unwrapped angle θ_0^{fp} .
287 Analyzing the shape and curvature of these spoke-like
288 aberrations can therefore provide valuable insights into
289 the underlying machine kinematics and support process
290 optimization.

291 **7. Summary**

292 This paper presents a set of graphical visualization
 293 methods for results obtained from a Zernike approxi-
 294 mation of wavefront aberrations or surface figure errors.
 295 These representations are intended to provide an intuitive
 296 visualization of the extensive information contained in the
 297 RMS-normalized Zernike coefficient vector. In particular,
 298 dominant characteristics are intended to be rapidly rec-
 299 ognized and extracted.

300 Zernike bubble charts are well suited for represent-
 301 ing low-order aberrations up to the 10th or 12th order.
 302 The area of each bubble is scaled according to the RMS
 303 value of the corresponding Zernike aberration, such that
 304 the relative scaling has a clear physical meaning. These
 305 bubble charts are particularly valuable when rapid vi-
 306 sual feedback on individual aberration terms is required,
 307 for example during aberration compensator adjustment,
 308 real-time wavefront visualization of dynamic processes,
 309 or optical alignment procedures. In addition, they can
 310 improve the clarity and interpretability of inspection re-
 311 ports or measurement certificates for lenses and optical
 312 systems.

313 Zernike heatmaps, by contrast, are well suited for rep-
 314 resenting mid- and high-spatial-frequency errors. For this
 315 purpose, the magnitude of the RMS-normalized coeffi-
 316 cients is displayed on a logarithmic scale in order to en-
 317 hance the visibility of contributions with small ampli-
 318 tudes. Such heatmaps reveal characteristic manufacturing
 319 artifacts, such as spoke-like structures or ripple patterns.

320 Furthermore, this work introduces an alternative def-
 321 inition of the azimuthal orientation of Zernike terms for
 322 $m \neq 0$. This approach enables the identification of the
 323 shape and bending of spoke-like aberrations. For such spe-
 324 cific analyses, other numerical methods, such as Fourier-
 325 based filtering or multi-angle averaging, may also be em-
 326 ployed [11]. However, given the availability of convenient
 327 numerical methods for fitting wavefronts or aberrations
 328 to very high Zernike orders [12], these features can now
 329 be directly extracted from the Zernike coefficients them-
 330 selves.

331 **Funding**

332 This research did not receive any specific funding.

333 **Conflict of Interest**

334 The author declares no conflicts of interest.

335 **Data Availability Statement**

336 The data that support the findings of this study are
 337 available from the corresponding author upon reasonable
 338 request. The MATLAB[®] code for visualizing Zernike co-
 339 efficients (bubble charts, heatmaps, and angular orienta-
 340 tion) will be made publicly available on the MATLAB[®]
 341 File Exchange.

Author Contribution Statement

342

This work was conducted and written solely by the 343
 author, who is fully responsible for all contributions and 344
 content. 345

References

346

1. Zernike F, Beugungstheorie des Schneidverfahrens und 347
 seiner verbesserten Form, der Phasenkontrastmethode, 348
Physica **1**(7), 689–704 (1934). [https://doi.org/10.1016/](https://doi.org/10.1016/S0031-8914(34)80259-5) 349
[S0031-8914\(34\)80259-5](https://doi.org/10.1016/S0031-8914(34)80259-5) 350
2. Malacara D (ed.), *Optical Shop Testing*, 2nd edn. (John 351
 Wiley & Sons, New York, 1992) [https://doi.org/10.1002/](https://doi.org/10.1002/9780470135976) 352
[9780470135976](https://doi.org/10.1002/9780470135976) 353
3. Gross H, Dörband B, Müller H (eds.), *Handbook of Optical* 354
Systems, Volume 5: Metrology of Optical Components and 355
Systems, 1st edn. (Wiley-VCH, Weinheim, 2012) [https://doi.org/10.1002/](https://doi.org/10.1002/9783527699230) 356
[9783527699230](https://doi.org/10.1002/9783527699230) 357
4. Niu K, Tian C, Zernike polynomials and their applica- 358
 tions, *J. Opt.* **24**(12), 123001 (2022). [https://doi.org/10.](https://doi.org/10.1088/2040-8986/ac9c88) 359
[1088/2040-8986/ac9c88](https://doi.org/10.1088/2040-8986/ac9c88) 360
5. Born M, Wolf E, *Principles of Optics*, 7th (expanded) edn. 361
 (Cambridge University Press, Cambridge, 1999) 362
6. Evans CJ, Parks RE, Sullivan PJ, Taylor JS, Visualization 363
 of surface figure by the use of Zernike polynomials, *Appl.* 364
Opt. **34**(34), 7815–7819 (1995). [https://doi.org/10.1364/](https://doi.org/10.1364/AO.34.007815) 365
[AO.34.007815](https://doi.org/10.1364/AO.34.007815) 366
7. Reichelt S, Pruss C, Tiziani HJ, Absolute interferomet- 367
 ric test of aspheres by use of twin computer-generated 368
 holograms, *Appl. Opt.* **42**(22), 4468–4479 (2003). [https://doi.org/10.1364/](https://doi.org/10.1364/AO.42.004468) 369
[AO.42.004468](https://doi.org/10.1364/AO.42.004468) 370
8. Webber JBW, A bi-symmetric log transformation for 371
 wide-range data, *Meas. Sci. Technol.* **24**(2), 027001 372
 (2013). <https://doi.org/10.1088/0957-0233/24/2/027001> 373
9. Forbes GW, Fitting freeform shapes with orthogonal 374
 bases, *Opt. Express* **21**(16), 19061–19081 (2013). [https://doi.org/10.1364/](https://doi.org/10.1364/OE.21.019061) 375
[OE.21.019061](https://doi.org/10.1364/OE.21.019061) 376
10. Hosseinimakarem Z, Davies AD, Evans CJ, Zernike poly- 377
 nomials for mid-spatial frequency representation on opti- 378
 cal surfaces, *Proc. SPIE* **9961**, 9961–18 (2016). [https://doi.org/10.1117/](https://doi.org/10.1117/12.2238514) 379
[12.2238514](https://doi.org/10.1117/12.2238514) 380
11. Reichelt S, Decomposition of non-rotationally symmet- 381
 ric wavefront aberrations into their azimuthal orders, in 382
Applied Optical Metrology III, ed. by Novak E, Trolinger 383
 JD, *Proc. SPIE* **11102**, 63–75 (2019). [https://doi.org/10.](https://doi.org/10.1117/12.2526938) 384
[1117/12.2526938](https://doi.org/10.1117/12.2526938) 385
12. Fan Y, Forbes GW, Rolland JP, Fast Zernike fitting 386
 of freeform surfaces using the Gauss-Legendre quadra- 387
 ture, *Opt. Express* **32**(11), 20011–20023 (2024). [https://doi.org/10.1364/](https://doi.org/10.1364/OE.498096) 388
[OE.498096](https://doi.org/10.1364/OE.498096) 389